Myocardial aging as a T-cell–mediated phenomenon

Gustavo Campos Ramos[a,b,1], Anne van den Berg[b], Vânia Nunes-Silva[c], Johannes Weirather[b], Laura Peters[b], Matthias Burkard[b], Mike Friedrich[d], Jürgen Pinnecker[d], Marco Abeßer[e], Katrin G. Heinze[d], Kai Schuh[e], Niklas Beyersdorf[f], Thomas Kerkau[f], Jocelyne Demengeot[c], Stefan Frantz[a,b,2], and Ulrich Hofmann[a,b,2]

[a]Department of Internal Medicine III, University Clinic Halle, D-06120 Halle, Germany; [b]Comprehensive Heart Failure Center, University Clinic Wuerzburg, D-97078 Wuerzburg, Germany; [c]Instituto Gulbenkian de Ciência, PT-2781-901 Oeiras, Portugal; [d]Rudolf Virchow Center for Experimental Biomedicine, University of Wuerzburg, D-97080 Wuerzburg, Germany; [e]Institute of Physiology I, University of Wuerzburg, D-97070 Wuerzburg, Germany; and [f]Institute for Virology and Immunobiology, University of Wuerzburg, D-97078 Wuerzburg, Germany

Edited by J. G. Seidman, Harvard Medical School, Boston, MA, and approved January 31, 2017 (received for review December 23, 2016)

In recent years, the myocardium has been rediscovered under the lenses of immunology, and lymphocytes have been implicated in the pathogenesis of cardiomyopathies with different etiologies. Aging is an important risk factor for heart diseases, and it also has impact on the immune system. Thus, we sought to determine whether immunological activity would influence myocardial structure and function in elderly mice. Morphological, functional, and molecular analyses revealed that the age-related myocardial impairment occurs in parallel with shifts in the composition of tissue-resident leukocytes and with an accumulation of activated $CD4^+$ $Foxp3^-$ (forkhead box P3) IFN-γ^+ T cells in the heart-draining lymph nodes. A comprehensive characterization of different aged immune-deficient mouse strains revealed that T cells significantly contribute to age-related myocardial inflammation and functional decline. Upon adoptive cell transfer, the T cells isolated from the mediastinal lymph node (med-LN) of aged animals exhibited increased cardiotropism, compared with cells purified from young donors or from other irrelevant sites. Nevertheless, these cells caused rather mild effects on cardiac functionality, indicating that myocardial aging might stem from a combination of intrinsic and extrinsic (immunological) factors. Taken together, the data herein presented indicate that heart-directed immune responses may spontaneously arise in the elderly, even in the absence of a clear tissue damage or concomitant infection. These observations might shed new light on the emerging role of T cells in myocardial diseases, which primarily affect the elderly population.

myocardial | aging | T cells | inflammation | inflammaging

The myocardial cellular composition has been revisited in recent years, and leukocyte subsets residing in the healthy heart have been described (1–10). Cardiac-resident macrophages exhibiting an M2-like gene expression profile were found to be distributed in close association with the coronary vascular bed (3), and niches for dendritic cells ($CD11c^+$ MHC-II^{high} $CD80/86^{low}$) were found near the cardiac valves of the intact heart (1). It was also demonstrated that cardiac-resident $MHCII^+$ cells process and present myosin heavy chain-alpha–derived peptides under steady-state conditions (11, 12) and prime T cells ex vivo (1). However, whether lymphocytes can seed the intact myocardium and whether T-cell priming with myocardial antigens can occur in the absence of an infection or autoimmune myocarditis remain elusive.

More recently, accumulating evidence indicated that noninfectious myocardial diseases are modulated by T cells. During the last couple of years, our group demonstrated that ischemic, sterile myocardial injuries can elicit lymphocyte activation directed against cardiac antigens (13–16). Our previous data, showing for the first time that $CD4^+$ T cells reactive to cardiac components can foster the healing process that takes place after myocardial infarction, were corroborated by several other reports (13, 15, 17–20). However, these autoreactive T cells can also be potentially deleterious (21). Furthermore, it has now been reported that even transverse aortic constriction (TAC) can induce T-cell responses, which in turn contribute to the development of heart failure (22, 23). The participation of T cells in this context is surprising because the TAC model induces chronic pressure-overload stress with minimal tissue injury.

Aging is another relevant situation in which local lymphocyte activity could affect cardiac structure and function. Myocardial senescence is associated with alterations in loading stress conditions, fibrosis, and cardiac functional impairment (24, 25). Furthermore, myocardial senescence is associated with cardiomyocyte cell death, leading to increased exposure of heart-specific antigens to immune cells (26). From the immunological perspective, aging is accompanied by an increased systemic inflammatory basal tone (27–29) and with defective maintenance of immunological tolerance (30–32).

These lines of evidence indicate that the heart is an immunologically active site, even under basal conditions, and that lymphocytes can sense shifts in cardiac functioning and eventually mount a local immune response. This finding prompted us to speculate that the cardiac and immunological alterations that are typically seen in elderly patients are intertwined events. Thus, in the present study, we set out (*i*) to characterize the lymphoid cells found in the myocardium and heart-draining lymph nodes of healthy (unimmunized/uninfected) mice at different ages and (*ii*) to investigate in which ways the activity of such lymphocytes could influence the myocardial aging process.

Significance

Aging is a risk factor for heart diseases, and it is also known to impact on several immunological processes. Nevertheless, most studies addressing the cardio-immune cross-talk have focused on juvenile rather than senescent animal models. In the present study, we addressed this gap and found that immunological activity contributes to myocardial aging. By using different lymphocyte-deficient animal models and heterochronic adoptive cell-transfer protocols, our study revealed a pivotal role for $CD4^+$ T cells in mediating spontaneous local inflammation and mild organ dysfunction in aged hearts. These results might shed new light on the emerging field of "immunocardiology" because they reveal that spontaneous heart-directed immune responses arise even in the absence of previous myocardial tissue damage.

Author contributions: G.C.R., V.N.-S., J.D., S.F., and U.H. designed research; G.C.R., A.v.d.B., V.N.-S., J.W., L.P., M.B., M.F., J.P., and M.A. performed research; K.G.H., J.D., S.F., and U.H. contributed new reagents/analytic tools; G.C.R., A.v.d.B., V.N.-S., J.W., L.P., M.F., J.P., M.A., K.S., N.B., T.K., J.D., S.F., and U.H. analyzed data; and G.C.R., K.G.H., K.S., N.B., T.K., J.D., S.F., and U.H. wrote the paper.

The authors declare no conflict of interest.

This article is a PNAS Direct Submission.

Freely available online through the PNAS open access option.

[1]To whom correspondence should be addressed. Email: gustavo.ramos@uk-halle.de.

[2]S.F. and U.H. contributed equally to this work.

This article contains supporting information online at www.pnas.org/lookup/suppl/doi:10.1073/pnas.1621047114/-/DCSupplemental.

Results

The Myocardium Harbors All Major Leukocyte Populations in the Steady State. Flow cytometry analysis of cell suspensions obtained from perfused–digested murine hearts (2 to 3 mo old) revealed the presence of all major leukocyte populations within the healthy myocardium (Fig. 1 *A*–*C*). After gating on single cells, the cardiac leukocytes (defined as $CD45^+$ cells) were further differentiated as monocyte/macrophages (defined as $CD45^+$ $CD11b^+$ $Ly6G^-$), granulocytes ($CD45^+$ $CD11b^+$ $Ly6G^+$), B cells ($CD45^+$ $CD11b^-$ $Ly6G^-$ $B220^+$), and T cells ($CD45^+$ $CD11b^-$ $Ly6G^-$ $CD3\varepsilon^+$). Using a bead-based strategy to obtain absolute cell numbers, we observed that our current protocol enabled the recovery of approximately 10^3 leukocytes per milligram of tissue in the steady state (macrophages, 567 ± 71 cells per milligram of tissue; B cells 160 ± 23 cells per milligram of tissue; T cells, 41 ± 5 cells per milligram of tissue; and granulocytes, 18 ± 3 cells per milligram of tissue) (Fig. 1 *E* and *F*). Of note, after applying the same cell-harvesting protocol to different muscle preparations, we observed that the cardiac muscle harbors 12-fold more leukocytes per milligram of tissue than the skeletal muscle (Fig. 1*D*).

To assess whether these leukocytes were located in contact with the coronary circulation or in the myocardial parenchyma, we performed intravascular (in an isolated–perfused heart system) and postdigestion staining using anti-CD45 antibodies coupled to different fluorochromes (Fig. S1*A*). We found that only ∼13% of cardiac leukocytes were in direct contact with the bloodstream. The parenchymal distribution of most cardiac leukocytes was further confirmed using histological approaches (Fig. S1*B*).

Considering that cell loss is expected to happen during the heart digestion and staining protocol, we used the light-sheet fluorescence microscopy (LSFM) approach to scan unsliced whole hearts and obtain a more accurate picture of the absolute cell number of cardiac leukocytes (Fig. 1 *G* and *H* and Movie S1). This approach enabled us to generate 3D reconstructions spanning large areas of intact myocardium and confirmed an abundant leukocyte distribution in hearts harvested from healthy, nonmanipulated animals (3,380 ± 1,279 $CD45^+$ cells per cubic millimeter of tissue).

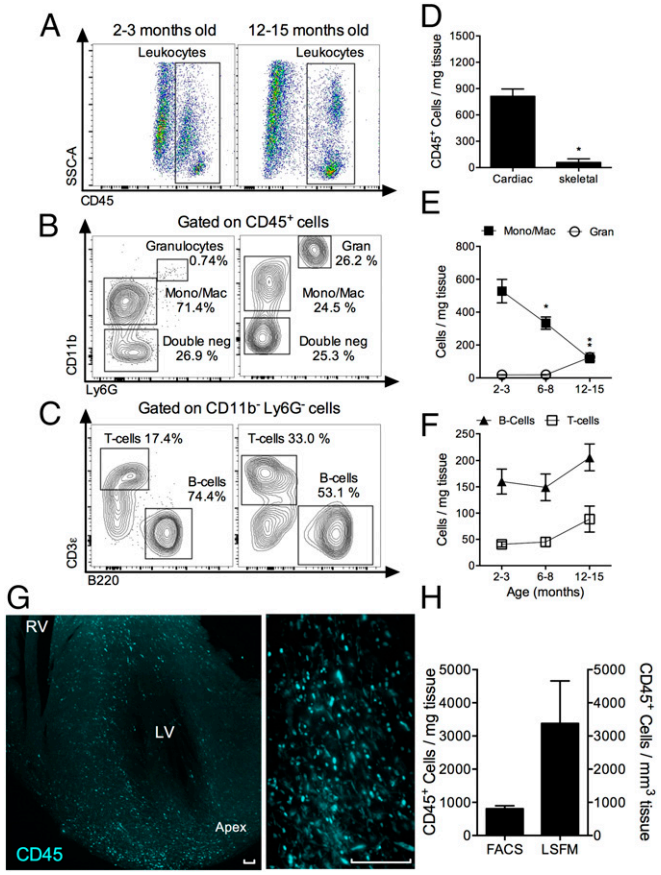

Fig. 1. Leukocyte populations found within the healthy myocardium. Cell suspensions obtained from perfused/digested hearts of 2- to 3-mo-old or 12- to 15-mo-old (*A*–*C*) animals were used for flow cytometry. The major leukocyte populations were defined as follows: monocytes/macrophages (Mono/Mac) ($CD45^+$ $CD11b^+$ $Ly6G^-$), granulocytes (Gran.) ($CD45^+$ $CD11b^+$ $Ly6G^+$), B cells ($CD45^+$ $CD11b^-$ $Ly6G^-$ $B220^+$), and T cells ($CD45^+$ $CD11b^-$ $Ly6G^-$ $CD3e^+$). (*D*) The same tissue digestion protocol was applied to cardiac and skeletal muscle samples under steady-state conditions, revealing a more abundant leukocyte presence within the healthy myocardium. The temporal fluctuations in the absolute cell counts of each subset are represented in *E* and *F*, where ■ represents monocyte/macrophages, ○ represents granulocytes, □ represents T cells, and ▲ represents B cells. (*G*) Entire hearts from healthy animals were stained with anti-CD45 antibodies and prepared for light-sheet fluorescence microscopy (LSFM). A Z-stack reconstruction spanning large myocardial areas in the longitudinal axis shows abundant resident leukocyte populations (*Left*, 150-μm Z axis, 5× magnification; *Right*, 1.5-mm *z* axis, 26× magnification). (Scale bars: 50 μm.) (*H*) The cardiac-resident leukocyte ($CD45^+$) cell numbers detected either using a tissue digestion–flow cytometry protocol or directly using LSFM were compared. The graphs represent the mean ± SEM of four to eight animals. Statistical tests performed were as follows: *t* test (bar graphs) and one-way ANOVA, followed by Dunnett's post hoc test comparing the same cell subset at different time points (line graphs). $*P < 0.05$; in *E*, ** shows that $*P < 0.05$ for both of the overlapping Mono/Mac and Gran lines. Data were pooled from at least two independent experiments. LV, left ventricle; RV, right ventricle.

Myocardial Aging Is Accompanied by Important Shifts in Resident Leukocyte Composition. Next, we analyzed the myocardial tissues obtained from 2- to 3-mo-old mice (from here on, termed young animals), 6- to 8-mo-old mice (adult animals), and 12- to 15-mo-old mice (aged animals) and found that important changes in cardiac leukocyte composition occur over time (Fig. 1 *E* and *F* and Fig. S2). The macrophage population (primarily $CD206^+$ cells) significantly decreased with aging, in parallel with an increase in the granulocyte infiltration (Fig. 1*E*). Despite the clear changes in macrophage absolute cell numbers, the frequencies of the $F4/80^+CD206^+$ and $F4/80^+CD206^-$ subsets remained unaltered with aging (Fig. S2 *A* and *B*). Still, a slight increase in the CCR2 (C-C motif chemokine receptor 2) expression on cardiac macrophages was observed in 12- to 15-mo-old animals, indicating a possible replenishment of resident macrophages by monocyte-derived-cells (Fig. S2 *C* and *D*). Both T- and B-cell numbers remained constant over time (Fig. 1*F*). No major age-related alteration in the cardiac B-cell compartment was observed when these cells were phenotyped based on the IgD/IgM expression (Fig. S2*F*). Within the cardiac T-cell subsets, the CD4:CD8 ratio was decreased in aged animals (Fig. S2*I*).

The age-related shifts in the composition of heart-associated leukocyte populations occurred together with myocardial functional and structural alterations (Fig. 2). Echocardiographic studies revealed an age-related decrease in fractional shortening (FS) (young animals FS, 63.76 ± 1.35% vs. aged animals, 51.24 ± 2.62%, $P < 0.05$), an increase in end-diastolic area (EDA) (young animals EDA, 7.43 ± 0.41 mm vs. aged animals, 9.93 ± 0.34 mm, $P < 0.05$), and an increase in end-diastolic anterior wall thickness (EDWT) (young animals EDWT, 0.067 ± 0.002 mm vs. aged animals, 0.086 ± 0.004 mm, $P < 0.05$) (Fig. 2 *A*–*E*). Of note, 15.7% of aged mice presented FS of <40%, which is considered to be a clinically significant phenotype. Similar findings were observed when cardiac function was assessed using a pressure-volume conductance catheter positioned in the left ventricle (Fig. S3).

Together with functional impairment, myocardial fibrosis and hypertrophy were observed in senescent hearts. Histological

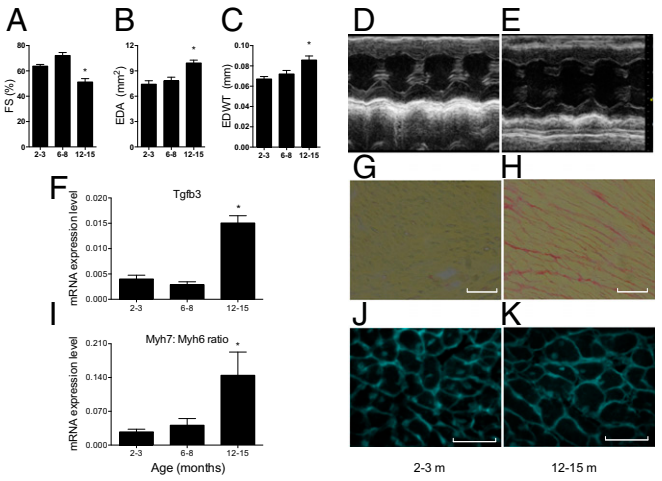

Fig. 2. Myocardial aging. Cardiac function, fibrosis, and hypertrophy were assessed over a 15-mo period. (*A–E*) Echocardiographic analysis revealed some age-related alterations in cardiac function and structure, including a mild reduction in fractional shortening (*A*), an increased end diastolic area (*B*), and an increase in end-diastolic anterior wall thickness (*C*). (*D* and *E*) Representative echocardiographic registers from young (2 to 3 mo old) and aged (12 to 15 mo old) mice, respectively. (*F*) The myocardial gene expression levels of *Tgfb3*. (*G* and *H*) Representative pictures of young and aged heart slices stained with Picrosirius red (PSR). (Scale bars: 50 μm.) (*I*) The ratio of the myocardial gene expression levels of myosin heavy chain isoforms 6 (alpha, cardiac) and 7 (beta, muscle). (*J* and *K*) Representative pictures of young and aged WGA-stained heart slices, respectively. The bar graphs represent the mean ± SEM of 5 to 19 animals (*A*) or 4 to 8 animals (*F* and *I*). The statistical test performed was as follows: one-way ANOVA followed by Dunnett's post hoc test. $*P < 0.05$ in comparison with young controls. Data are pooled from at least two independent experiments.

analysis revealed increased interstitial collagen deposition (Fig. 2 *G* and *H*) and cardiomyocyte cross-sectional area over time (Fig. 2 *J* and *K* and Fig. S3*D*). Furthermore, the expression levels of profibrotic (Fig. 2*F*) and prohypertrophic genes (Fig. 2*I*) were also increased in senescent hearts.

Age-Related Cardiac Functional Decline Is Associated with Increased in Situ Inflammation. To further assess the age-related alterations in the myocardial molecular milieu, we designed a custom quantitative PCR (qPCR) array to probe the expression levels of 45 target genes (and 3 endogenous controls) that reflect different aspects of cardiomyocyte biology, inflammation, angiogenesis, and fibrosis. Accordingly, we found that genes related to inflammation (e.g., *Tnf*, tumor necrosis factor), monocyte recruitment (e.g., *Ccl2*, C-C motif chemokine ligand 2), and cell stress (*Hspa1a*, heat shock protein family A member 1A) were up-regulated in the myocardial tissues obtained from 12- to 15-mo-old mice compared with young WT animals (Fig. 3). The expression levels of genes classically related to adaptive immunity were also up-regulated in the aged myocardium (e.g., *Ifng*, interferon γ; and *Cxcl13*, C-X-C motif chemokine ligand 13), suggesting that lymphocytes might play a special role in the myocardial aging process (Fig. 3*A*). The main PCR array results were further confirmed using a standard qPCR approach, with additional biological and technical replicates (Fig. 3 *B–G*).

In an attempt to delineate the sequence of events that lead to myocardial aging, we assessed the expression levels of key genes that are responsive to different stress contexts. Shifts in the expression of *Gata4* (GATA-binding protein 4), which is a cardiomyocyte transcription factor that is responsive to loading stress conditions, were the earliest alteration seen in the myocardium, occurring in animals aged 6 to 8 mo old. Only at later time points (12 to 15 mo) were the expression levels of genes related to redox stress (*Sirt1*, sirtuin 1), inflammation (*Tnf, Ifng*), and other stress conditions (*Hspa1a*) found to be up-regulated. No alterations in myocardial *Hif1a* (hypoxia-inducible factor 1 alpha subunit) expression levels were observed with aging, suggesting that myocardial senescence is not mediated by hypoxic stress.

Spontaneous CD4$^+$ T-Cell Activation Occurs in the Mediastinal Lymph Nodes of Aged Mice. The observation that age-related cardiac functional and structural impairment occurs in parallel with increased myocardial expression of genes related to the adaptive immune response prompted us to investigate whether lymphocyte activity plays a role in myocardial aging. Thus, we next characterized the heart-draining (mediastinal) lymph nodes (med-LNs) of young and aged mice under steady-state conditions. As controls, we used the popliteal lymph nodes (pop-LN) because they drain primarily the hind limb skeletal muscle (Fig. 4 and Figs. S4 and S5).

Surprisingly, we observed that aging was accompanied by an increased cellularity in the heart-draining LNs, but not in the pop-LNs (Fig. 4*A*), suggesting that local immune-inflammatory activity might occur in the senescent hearts. Naive 12- to 15-mo-old animals presented a stark increase in the frequency of CD4$^+$ T cells with an activated or effector-memory phenotype (CD44^{high} CD62^{low}) (Fig. 4 *B* and *C*) in both lymph node stations in comparison with young controls (med-LN young, 13.8 ± 1.1% of CD44^{high} CD62^{low} among CD4$^+$ T cells; med-LN aged, 36.1 ± 1.9% of CD44^{high} CD62^{low} among CD4$^+$ T cells, $P < 0.05$).

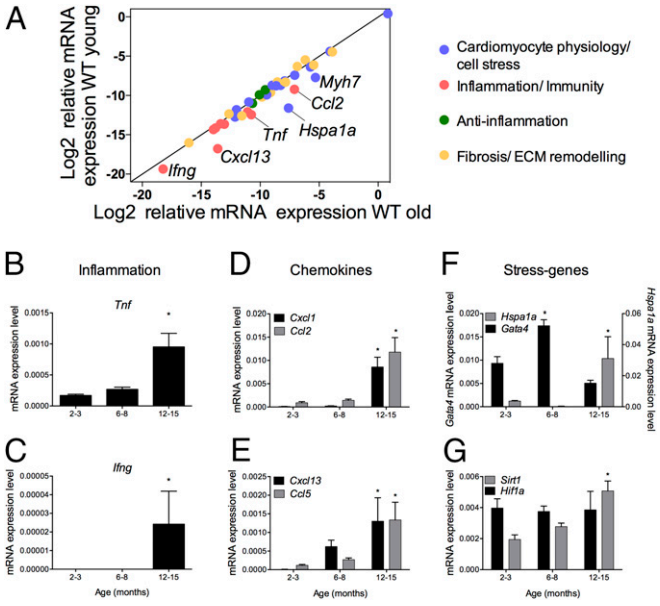

Fig. 3. Cardiac aging and inflammation. (*A*) Scatter plot comparing the normalized myocardial gene expression levels (Log2 relative gene expression) of naive WT young (2 to 3 mo old) versus aged (12 to 15 mo old) mice. A custom-made PCR array including 45 genes related to cardiomyocyte responses to cell stress (blue dots), inflammation (red dots), antiinflammation (green dots), and extracellular matrix (ECM) biology (yellow dots) was designed, and pooled myocardial samples were tested ($n = 3$ per group). Next, the most relevant genes related to inflammation (*B–E*) and cell stress (*F* and *G*) were further tested individually with additional biological and technical replicates. The bar graphs represent the mean ± SEM of three to six animals. The statistical test performed was as follows: one-way ANOVA followed by Dunnett's post hoc test. $*P < 0.05$ in comparison with young controls. The qPCR-arrays were performed as a single experiment whereas the standard qPCR reactions were performed using samples from at least two independent experiments.

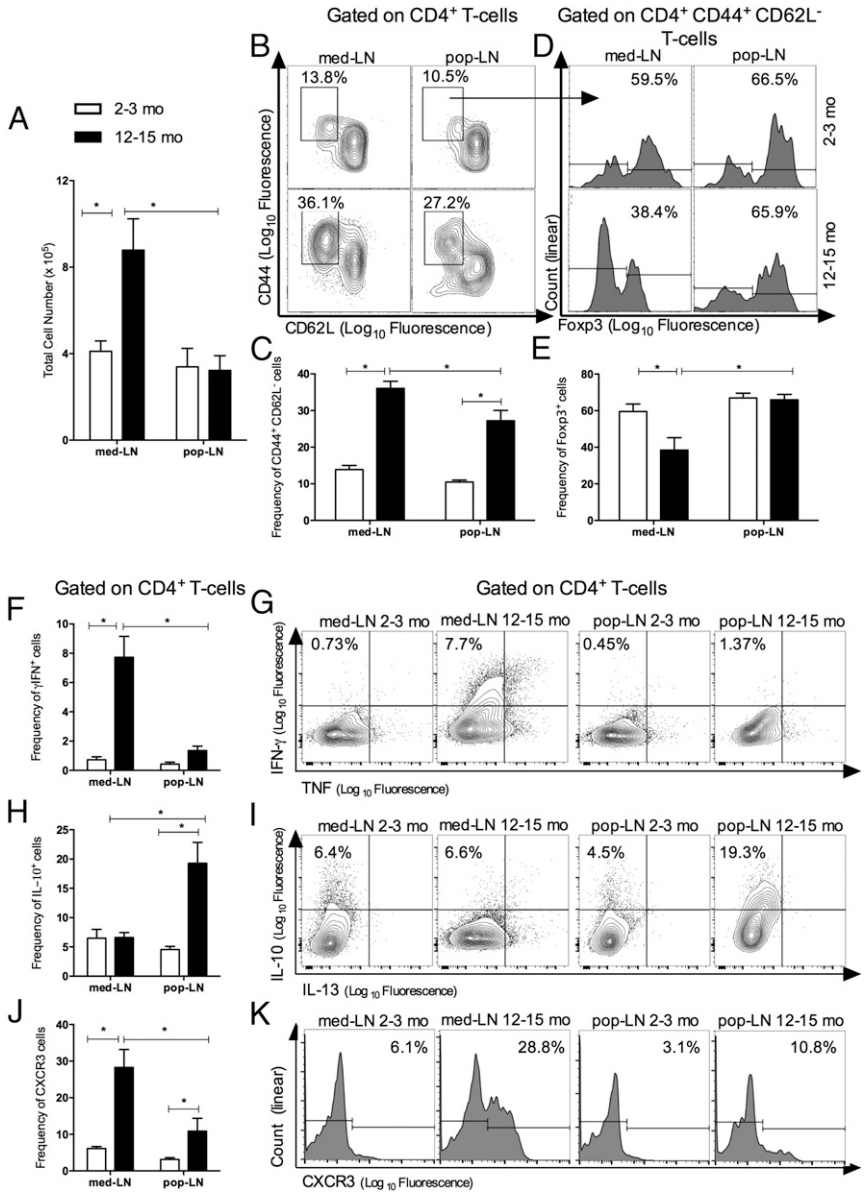

Fig. 4. Analysis of the heart-draining lymph nodes during aging. (*A*) Absolute cell number per lymph node station. Flow cytometry analysis revealed an age-related accumulation of CD44^{high} CD62L^{low} CD4^{+} T cells (i.e., activated, effector/memory phenotype) in both the popliteal and mediastinal lymph nodes although the accumulation was more evident in the mediastinal lymph nodes (*B* and *C*). The frequency of Foxp3^{+} cells among the CD44^{high} CD62L^{low} CD4^{+} T cells was significantly reduced in mediastinal but not popliteal LN from aged animals (*D* and *E*). Upon in vitro stimulation with PMA plus ionomycin, the CD4^{+} T cells harvested from the aged mediastinal LN preferentially produced IFNγ (*F* and *G*) whereas the cells isolated from the popliteal LN (same animals) produced IL-10 (*H* and *I*). Alongside with the IFN-γ expression pattern, the surface expression of the chemokine receptor CXCR3 was preferentially up-regulated in the CD4^{+} T cells found in the med-LN of aged animals (*J* and *K*). The bar graphs represent the mean ± SEM of five to eight animals. The statistical test performed was as follows: two-way ANOVA followed by the Tukey post hoc test. *$P < 0.05$, as indicated in the graphs.

However, the accumulation of such effector T cells was more pronounced in the med-LN than in the age-matched pop-LN (pop-LN aged, 27.2 ± 2.85% CD44^{high} CD62^{low} among CD4^{+} T cells; $P < 0.05$, compared with age-matched med-LN). Furthermore, important shifts in the Treg [regulatory T cells, CD4^{+} Foxp3^{+} (forkhead box P3)]:Tconv (conventional T cells, CD4^{+} Foxp3^{-}) ratio were observed in the med-LN of aged mice (Fig. 4 *D* and *E*). Although the majority of the antigen-experienced CD4^{+} T cells found in the med-LN of young healthy mice were Foxp3^{+}, the same T-cell compartment was primarily composed of Foxp3^{-} cells in elderly mice. A more detailed FACS analysis revealed that this shift was primarily caused by an accumulation of antigen-experienced conventional T cells (Foxp3^{-}), rather than a decrease in activated Foxp3^{+} (Fig. S4 *E* and *F*). In sharp contrast to the med-LN, no alterations in the Treg:Tconv ratio were observed in the pop-LN, where the majority of activated cells remained Foxp3^{+}, even in senescent animals (Fig. 4 *C* and *D*). For the sake of further comparing the age-related shifts seen in the med-LN with other LN sites, we also characterized the T-cell compartment in the subiliac LNs (si-LNs) of young and aged animals (Fig. S5). As in the pop-LN (and in sharp contrast with the med-LN), no age-dependent increase in cellularity was observed in si-LN. Furthermore, the age-dependent shifts in the surface expression levels of cell activation (CD44) and homing markers [CD62L, CXCR3 (C-X-C motif chemokine receptor 3)] on T cells in the si-LN were more similar to what was seen for

the pop-LN rather than for the med-LN (Fig. S5). These results reinforce the notion that regional-specific shifts in the med-LN arise with aging.

When stimulated in vitro with phorbol 12-myristate 13-acetate (PMA) plus ionomycin, the $CD4^+$ T cells harvested from the aged med-LN produced primarily IFN-γ (Fig. 4 *F* and *G*) whereas the cells harvested form the pop-LN exhibited a preferential IL-10 response (Fig. 4 *H* and *I*). IL-13 was hardly detectable in T cells. Alongside with the IFN-γ expression pattern, the surface expression of CXCR3, a chemokine receptor primarily expressed on Th1 cells, was also preferentially up-regulated on the $CD4^+$ T cells found in the med-LN of aged animals (Fig. 4 *J* and *K*). Similar findings were observed for $CD8^+$ cells (Fig. S6).

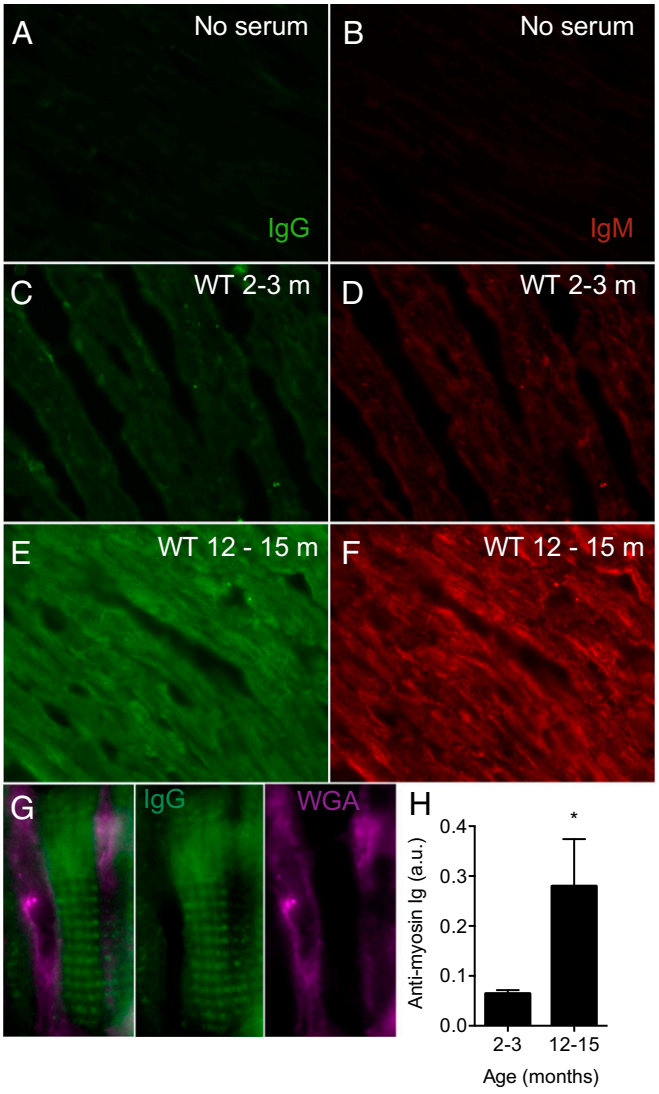

Fig. 5. Spontaneous heart-directed autoreactivity arises with aging. Heart-specific autoantibodies were detected by means of incubating the plasma of young/aged animals with histological heart slices prepared from B-cell–deficient animals (thus, with no endogenous immunoglobulins). IgGs reacting against cardiac antigens are depicted in green (*A*, *C*, *E*, and *G*) whereas autoreactive IgMs appear in red (*B*, *D*, and *F*). (*A* and *B*) Control heart slides incubated with secondary antibodies only (no plasma). *C* and *D* show heart-specific autoreactivity found in young animals' plasma whereas *E* and *F* show autoreactivity found in aged animals. (*G*) Higher magnification showing that most IgGs that spontaneously arise with aging target sarcomeric antigens. (*H*) Myosin-specific antibodies. The bar graph represents the mean ± SEM of six to eight animals. The statistical test performed was as follows: *t* test. $*P < 0.05$. (Magnification: *A*–*F*, 400×; *G*, 1,000×.)

Heart-Directed Autoreactivity Spontaneously Arises with Aging. The accumulation of IFN-γ–producing effector $CD4^+$ T cells in the med-LN prompted us to consider that autoimmune mechanisms could play a role in myocardial aging. Therefore, we measured the levels of heart-specific autoantibodies in the plasma of young versus aged animals. As seen in Fig. 5, IgMs and IgGs targeting cardiac antigens spontaneously arise with aging (Fig. 5 *A*–*G*). These heart-reactive autoantibodies mainly recognize intracellular sarcomere structures, but not cardiomyocytes' surface antigens (Fig. 5*G*). These findings were further confirmed by measurements of myosin-specific antibody titers (Fig. 5*H*). Because B cells rely on T-cell help to secrete IgGs, these findings indicate that both B-cell–dependent and $CD4^+$ T-cell–dependent heart-specific autoimmune mechanisms might occur in elderly mice.

Elderly CD4-Deficient and $Ova_{323–339}$–T-Cell Receptor Transgenic Mice Exhibited Attenuated Cardiac Inflammation and Dysfunction Compared with WT Mice. Next, we performed a comprehensive cardiac phenotyping of the following aged lymphocyte-deficient mouse strains: $CD4^+$ T-cell–deficient mice (CD4KO and MHC-IIKO), mice with $CD4^+$ T cells bearing a transgenic T-cell receptor (TCR) that recognizes an irrelevant peptide presented on MHC-II context ($ovalbumin_{323–339}$, OT-II mice), and B-cell–deficient mice (μMT). Of note, all those mouse strains are on the same genetic background and were housed under the same conditions.

Echocardiographic studies revealed that, in contrast to WT mice, elderly animals devoid of $CD4^+$ T cells (MHC-IIKO) presented preserved fractional shortening (FS aged WT, 51.24 ± 2.62%; age-matched MHC-IIKO, 61.66 ± 2.04%, $P = 0.05$) (Fig. 6*A* and Table S1) and end diastolic area (aged WT, 9.93 ± 0.34 mm; age-matched MHC-IIKO, 7.19 ± 0.46 mm, $P = 0.05$) (Fig. 6*B*). Of note, no aged MHC-IIKO mouse presented FS of <40% (in sharp contrast to WT mice). The age-related cardiac decline seemed to be specifically related to T cells because B-cell deficiency did not result in preserved cardiac function in elderly mice (μMT FS, 55.78 ± 3.51%; μMT EDA, 10.28 ± 0.57 mm, $P >$ 0.05 compared with WT mice).

To further understand how T-cell deficiency relates to the cardiac dysfunction seen in elderly mice, we used myocardial samples obtained from different immunodeficient mice to probe the expression levels of 45 target genes. Overall, myocardial samples obtained from age-matched CD4-deficient or MHC-II–deficient animals showed reduced expression levels of proinflammatory genes (e.g., *Tnf,* and *Il1b*), compared with age-matched WT animals (Fig. 6 *C* and *D*). Although both mouse strains are characterized by a deficiency in $CD4^+$ T cells, the shifts in myocardial gene expression levels were more evident in the CD4KO strain. Furthermore, mice with $CD4^+$ T cells that bear a transgenic TCR with irrelevant specificity (OT-II animals) showed a similar reduction in inflammatory gene expression levels (Fig. 6*E*), indicating that autoantigen recognition by $CD4^+$ T cells might be important. In sharp contrast, B-cell–deficient animals (μMT) presented a myocardial gene expression profile nearly identical to that of age-matched WT animals (Fig. 6*F*), thus indicating that the age-related rise in the baseline levels of myocardial inflammation might be related to T cells' rather than B cells' activity. Based on the qPCR array data, some individual target genes were further probed with biological and technical replicates, allowing us to perform statistical analysis to validate the major findings (Fig. 6 *G*–*I*). Accordingly, we observed that CD4-deficient animals (but not B-cell–deficient) expressed lower *Tnf* levels in the myocardium, compared with age-matched WT animals (Fig. 6*G*), whereas the expression levels of *Myh7* (myosin

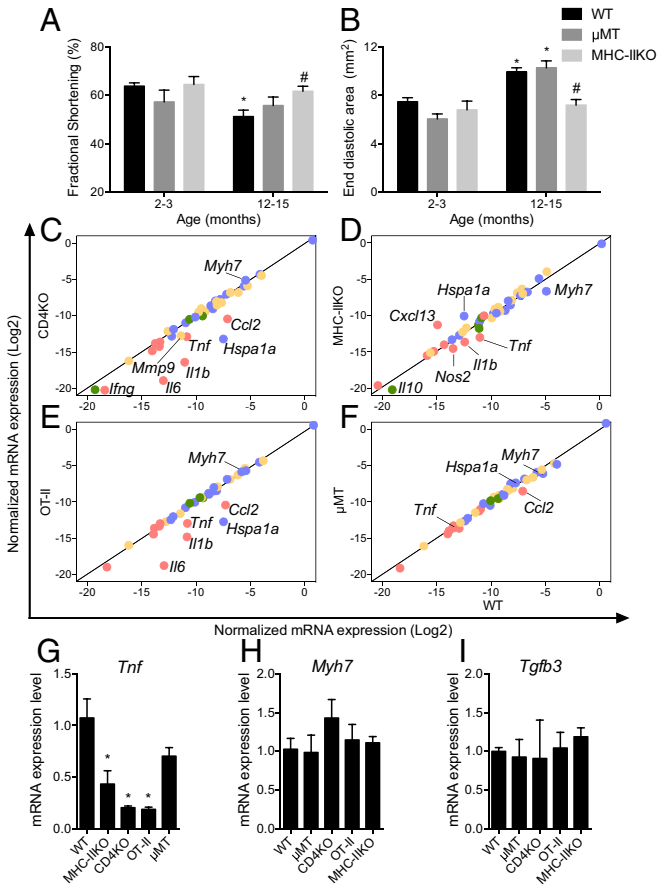

Fig. 6. Assessing the cardiac phenotype of different lymphocyte-deficient mouse strains. We performed a comprehensive cardiac phenotyping of 12- to 15-mo-old animals of the following mouse strains: CD4KO (CD4 deficiency), MHCIIKO (CD4 deficiency), OT-II (in which most of CD4+ T cells bear a transgenic TCR to an irrelevant pep-MHC), and μMT (B-cell deficiency). Echocardiographic analysis revealed that WT and B-cell–deficient mice, but not MHC-II–deficient mice, presented an age-related reduction in fractional shortening (*A*) and increase in end diastolic area (*B*). (*C–F*) A custom-made PCR array including three housekeeping genes and 45 genes related to cardiomyocyte responses to cell stress (blue dots), inflammation (red dots), antiinflammation (green dots), and extracellular matrix biology (yellow dots) was used to profile myocardial gene expression levels of different aged immunodeficient mice. Scatter plots of normalized gene expression levels (Log2 relative gene expression) comparing WT vs. CD4KO, WT vs. MHC-IIKO, WT vs. OT-II, and WT x μMT mouse strains are shown in *C–F*, respectively. PCR array data were further validated by performing qPCR reactions with individual samples for specific genes (*G–I*). The bar graphs represent the mean ± SEM of 5 to 19 animals (*A* and *B*) or 3 to 5 animals (*G–I*). The statistical test performed in *A* and *B* was as follows: two-way ANOVA followed by the Tukey post hoc test; $^{\#}P < 0.05$ compared with age-matched WT mice; $^{*}P < 0.05$ compared with genotype-matched young controls. The statistical test performed in *G–I* was as follows: one-way ANOVA followed by Dunnett's post hoc test; $^{*}P < 0.05$ compared with age-matched WT mice. The experiments including aged immunodeficient mouse strains were performed once using littermate controls.

heavy chain 7) and *Tgfb3* (transforming growth factor beta 3) remained unaltered.

Myocardial Aging as a Combination of Immune and Somatic Factors. To test whether lymphocytes residing in the heart-draining LN are sufficient to trigger the age-related myocardial alterations we evidenced above, we performed isogenic adoptive lymphocyte transfer into young lymphocyte-deficient animals (RagKO recipients). Donor cells (10^6 per recipient mice) were harvested from med-LN of young (2 to 3 mo old) or aged (12 to 15 mo old) WT animals ("YY" and "OY-med-LN" experimental groups, respectively). To control for the specificity of the putative alteration imposed by old med-LN, additional control groups received cells harvested from med-LN of aged lymphocyte-deficient donors (OY-med-LN-TCRβKO) or from the subiliac LN of aged WT donors (OY-si-LN).

Four months after adoptive cell transfer, T cells were detectable in the lymphoid organs of each recipient mouse that received cells from WT donors, confirming the success of engraftment (Fig. S7). The total leukocyte counts in the spleen were similar across experimental groups (approximately 4×10^6 cells) whereas LN cellularity was increased in animals receiving cells from young compared with old WT donors (Fig. S7), presumably the result of more vigorous lymphopenia-induced proliferation. As expected,

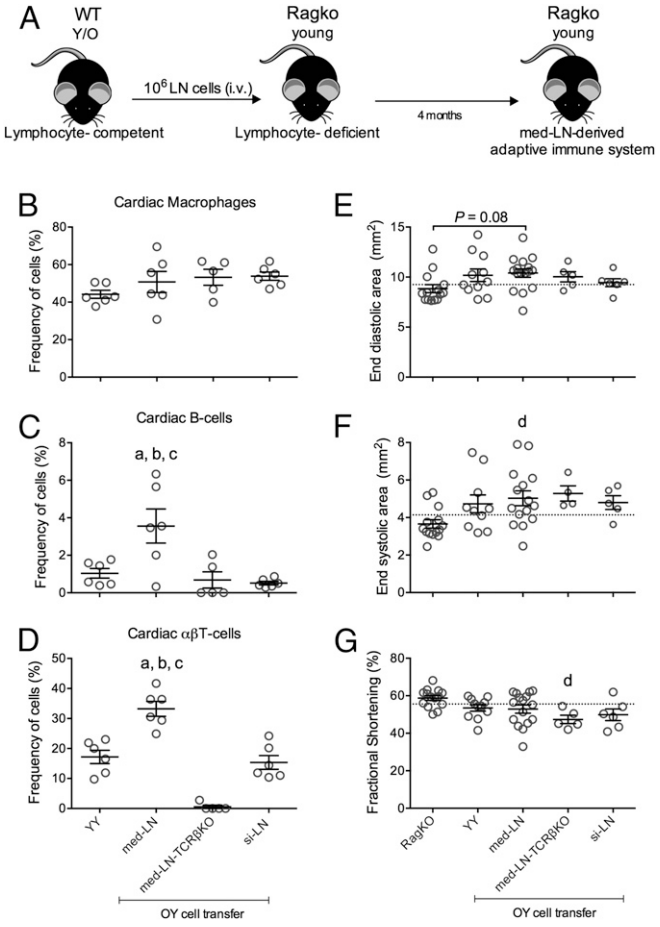

Fig. 7. Heterochronic lymphocyte adoptive cell transfer. Juvenile lymphocyte-deficient RagKO mice were adoptively transferred with med-LN cells from WT young (YY) or aged donors (OY-med-LN). Additional groups received cells purified from the med-LNs of aged T-cell–deficient donors (OY-med-LN-TCRβKO) or from the subiliac LN cells of aged WT donors (OY-si-LN) (*A*). (*B–D*) The frequencies of major cardiac leukocyte populations were determined by flow cytometry at 4 mo after cell transfer. Macrophages (*B*) were defined as $CD45^+$ $CD11b^+$ $Ly6G^-$; B cells (*C*) were defined as $CD45^+$ $CD11b^-$ $B220^+$; and alpha beta T cells (*D*) were defined as $CD45^+$ $CD11b^-$ $TCR\beta^+$. (*E* and *F*) Echocardiographic analysis performed at 4 mo after cell transfer. The dashed lines in *E* and *F* indicate the upper 95% confidence interval (CI) of age-matched RagKO controls, and the dashed line in *G* indicates the lower 95% CI of age-matched RagKO controls. The graphs show the individual values obtained from each mouse and the mean ± SEM of 5 to 16 mice. The statistical test performed was as follows: one-way ANOVA followed by the Tukey post hoc test. The letters "a," "b," and "c" represent $P < 0.05$ when the OY-med-LN group was compared with YY, OY-si-LN, and OY-med-LN TCRβKO, respectively. The letter "d" represents $P < 0.05$ compared with naive Ragko controls.

no $CD4^+$ or $CD8^+$ T cells were detected in mice recipient of TCRβKO donors (Fig. S7 *D–I*).

Strikingly, an assessment of the composition of cardiac tissue leukocytes revealed a clear dependency on age and origin of donor cells. The frequencies of myocardial T and B cells (but not that of macrophages) were significantly increased in the recipients that received cells isolated from the med-LN of old donors, compared with all other experimental groups (Fig. 7 *B* and *C*). This analysis also reveals that T cells are the major infiltrates of cardiac tissue under these conditions and that these exhibit an effector/memory phenotype (Fig. S7 *J–L*). By revealing the cardiotropism of T cells present in the med-LN of aged animals, these findings provide further evidence for a med-LN–heart immunological axis operating under baseline conditions in elderly mice.

Although exhibiting increased cardiotropism, the T cells isolated from the med-LN of aged donors had only minor specific effects on cardiac function. Expression levels of *Tnf*, *Myh7*, and *Tgfb3* were not significantly altered in any cell-transfer group (Fig. S8 *A–C*). Echocardiographic measurements indicated higher end-diastolic and end-systolic area in the animals of the OY-med-LN group, compared with RagKO control animals ($P = 0.08$ and $P < 0.05$, respectively), but not compared with other groups. Furthermore, the heart-to-body weight ratio was increased in 40% of the OY-med-LN mice (but not in other cell-transfer groups) (Fig. S8*D*). Intriguingly, animals that received med-LN cells isolated from αβ T-cell–deficient aged animals (TCRβKO) presented a reduction in fractional shortening, compared with RagKO control animals. Because these animals showed only minimal myocardial B-cell infiltration, and negligible levels of circulating myosin-specific antibodies, the echocardiographic alterations seen in this group most likely resulted from an enrichment in γδT cells. In support of this hypothesis, splenocytes purified from the OY-med-LN-TCRβKO animals produced high levels of IFN-γ and responded to anti-CD3 stimulation (Fig. S8*F*). These data suggest that, besides $CD4^+$ and $CD8^+$ T cells, other cells, such as γδT cells, might also influence the cardiac function under these experimental conditions.

From these heterochronic adoptive cell-transfer experiments, we conclude that T cells in the med-LN of old mice are poised to infiltrate heart tissues but do not cause, per se, major cardiac alterations. In turn, these data support a scenario whereby aged T cells are required, but not sufficient, to cause senescence-associated myocardial alterations.

Discussion

Presence of Lymphocytes in the Healthy Myocardium. Recent studies indicated that the murine myocardium harbors abundant tissue-resident macrophages and bona fide dendritic cells in the steady state (1–10). In the present study, we observed that a small population of B and T lymphocytes can also be consistently found in the myocardial parenchyma of healthy mice.

Although lymphocytes are best characterized in the blood, lymphatic fluid, and lymphoid organs, interest in tissue-resident lymphocytes is currently emerging (33–37). Different lymphocyte populations have now been described in several nonlymphoid organs, where they can influence the local molecular milieu and modulate other resident cells (38–41). For instance, Tregs found in the skeletal muscle can signal to local satellite (progenitor) cells and mediate tissue renewal (41) whereas conventional hippocampal T cells can modulate neuronal synapse plasticity (39). In the present study, we confirmed that the heart is not an exception and that lymphocytes indeed seed the myocardium under steady-state conditions.

Holzinger et al. (42) first reported the presence of antigen-experienced T cells ($CD3^+CD45RO^+$) within the noninfected/noninjured human myocardial parenchyma, but the methods used in that study did not permit a comprehensive characterization of those cells. Recently, Bönner et al. (2) used a flow cytometry approach to further demonstrate that, beyond the well-established resident macrophages, all major leukocyte populations can be found in heart samples obtained from healthy mice.

Our current study brings important advances to the emerging field of cardiac leukocytes. First and foremost, we used a refined imaging approach to obtain accurate cell numbers and tissue distribution patterns for cardiac $CD45^+$ cells. The challenges imposed by the low recovery of rare tissue-resident leukocytes have been a major factor in underestimating the relevance of such cells under basal conditions and hindering further advances in this field (35). Our 3D imaging studies of the intact heart confirmed that the $CD45^+$ resident population is larger than usually inferred using extraction-based methods. Furthermore, beyond a mere description of the heart-associated cells, we provided a comprehensive characterization of the cardiac phenotype in different immunodeficient mouse strains at steady state and during aging. The current study describes some of these immunodeficient transgenic mice at an advanced age (12 to 15 mo old). This innovation enabled us to dissect the role of lymphocytes in the myocardial aging process.

Myocardial Aging as a T-Cell–Mediated Phenomenon. Our data indicate that the myocardial and immunological aging processes are intertwined phenomena. It has been long recognized that myocardial aging is associated with increased interstitial fibrosis, hypertrophy, inflammation, stiffness, and mild contractile dysfunction (25). Several mechanisms have been proposed to explain this condition, including mitochondrial impairment (43), cardiomyocyte intrinsic factors (25), and deregulated immune responses (44–46).

In addition to affecting cardiac functionality, senescence also has a tremendous impact on immunological activity (27, 32, 47–49). Senescent mammals exhibit a progressive thymic involution that results in a stark reduction in naive T-cell production, the accumulation of antigen-experienced T cells, and repertoire skewing (32). Furthermore, aging is accompanied by reductions in thymic Treg production (49) and in the output of recent thymic emigrants, the preferential precursors of peripherally induced Tregs (50).

Smith and Allen (11) have previously reported that cardiac antigens can be constitutively presented to T cells under baseline conditions. Here, we report that physiological aging is accompanied by specific alterations in the heart-draining LNs, even in the absence of concomitant diseases. In summary, we report that the T cells found in the med-LN of aged animals exhibit a stronger type-1 response, compared with age-matched pop-LN cells, and increased cardiotropism. Furthermore, a comprehensive cardiac phenotyping of different aged lymphocyte-deficient mouse strains indicated that $CD4^+$ T cells are required for the myocardial aging process. Regional-specific shifts in the LN composition under basal conditions have been recently reported by independent groups. Peptidome and "degradome" analysis on the lymph self-antigen repertoire has revealed important regional-specific patterns across different LN stations, reflecting the composition of the drained tissue (51). Furthermore, Bergot et al. (52) found that the T cells' repertoire and differentiation status can vary across different LN sites, also depending on the nature of tissue being drained.

The data on heart-specific autoantibodies herein presented confirms that autoimmune mechanisms might underline the age-related shifts in the med-LN composition. Because the IgG production normally relies on $CD4^+$ T-cell help (53), those results reinforce that aging might trigger heart-specific B- and T-cell responses. Autoantibodies targeting cardiac antigens have been described in different heart failure conditions (54). These autoantibodies may have particular clinical relevance when targeting surface receptors important for cardiomyocytes' function (55). However, because most of the heart-specific antibodies

found in elderly mice seemed to target inaccessible intracellular antigens, we assume they might be a consequence of a life-long antigenic exposure, rather than agents that promote myocardial aging. The findings showing that aged B-cell–deficient animals (thus Ig-deficient) exhibit a myocardial aging phenotype comparable with age-matched WT controls further suggest that B cells and autoantibodies might not be pathogenic under these conditions. Still, we acknowledge that the significance of naturally occurring autoantibodies is far from being settled, and we hope our study could encourage further research to access the role of autoantibodies in myocardial health and disease.

In the present study we used an adoptive cell-transfer approach to assess the pathogenic potential of the med-LN cells at different time points. The cardiotropism displayed by the med-LN T cells of aged mice further supports the notion that the cells present in the med-LN can potentially influence the myocardial molecular milieu. Recently, Komarowska et al. (56) uncovered some molecular mechanisms conferring cardiotropism to T cells. They found that the myocardial tissue expresses hepatocyte growth factor (HGF), which is eventually drained to the med-LN, to be sensed by T cells, which express the HGF receptor c-met. In this elegant study, authors showed that T cells activated in the presence of HGF up-regulate the expression of CXCR3 and CCR4 chemokine receptors and home to the heart.

Whether the heart-directed immune activity is the trigger or the amplifier of the tissue damage associated with myocardial aging remains to be established although our data support the latter alternative. We observed that fluctuations in myocardial expression of *Gata4*, which is a gene involved in hypertrophy and responses to loading stress, precede the rise of a clear immune-inflammatory local response. Moreover, the differences in cardiac function across different cell-transfer protocols were rather moderate, suggesting that lymphocytes alone do not account for all of the alterations seen in the senescent hearts. Based on these findings, we put forward that myocardial aging might stem from a combination of both intrinsic (cardiac) and extrinsic (immunological) factors. Lymphocytes might therefore act as amplifying rather than creating the conditions leading to myocardial deterioration in the elderly. Our data suggest that they contribute to a state of low-grade myocardial inflammation that promotes the structural alterations in the myocardial tissue coming along with aging.

Last, but not least, although we have primarily focused on the role played by $CD4^+$ T lymphocytes in mediating myocardial aging, the participation of other inflammatory mechanisms might also be considered. For instance, Molawi et al. (9) reported that the cardiac resident macrophages (originally derived from the yolk sac) tend to be replenished by monocyte-derived cells with aging, even in the absence of tissue damage. Such monocyte-derived cardiac macrophages have been reported to hold higher proinflammatory potential, compared with their embryonic counterparts (5). Furthermore, Pinto et al. (57) reported that a profibrotic resident macrophage subset (defined as $CX3CR1^{low}$ $CD206^+$) arises in the myocardium of 30-wk-old animals. In the current study, we also expand these observations and report shifts in the myocardial myeloid compartment at advanced ages (in animals aged 12 to 15 mo old).

Concluding Remarks

By making use of targeted cell ablation (genetic models) and LN cell-transfer approaches, our study revealed that $CD4^+$ T cells mediate cardiac inflammation and mild functional impairment in elderly subjects, even in the absence of clear tissue damage or concomitant infection. The constitutive presence of T cells with reactivity to myocardial tissue deserves further consideration as a disease-modifying factor, especially in the clinical context of heart failure, which predominantly affects the elderly population. These observations might shed new light on the emerging role of T cells in myocardial diseases.

Materials and Methods

Animals. Naive male C57BL/6J (stock no. 000664) mice aged 2 to 15 mo were acquired from the Jackson Laboratory and housed under specific pathogen-free (SPF) conditions, with a controlled light–dark cycle and a standard diet. Myocardial aging was studied in naive animals aged 2 to 3 mo (regarded as young animals), 6 to 8 mo (adult animals), and 12 to 15 mo (aged animals). To investigate the role of different lymphocyte subsets in myocardial aging, we also characterized the following mouse strains (also from The Jackson Laboratory): CD4KO (T-helper cell–deficient; stock no. 002663), MHC-II–deficient (T-helper cell–deficient; stock no. 003584), OT-II (mice bearing a transgenic TCR recognizing the $Ova_{323–339}$ peptide in the context of $I\text{-}A^b$, an irrelevant antigen in the myocardial context; stock no. 004194), and μMT B-cell–deficient mice (stock no. 002288). All mouse strains included in this study are on the same genetic background (B6/J), and the appropriate WT control animals (C57BL/6J) were taken as suggested by The Jackson Laboratory.

Cell Transfer. Mediastinal lymph nodes (med-LNs) were isolated from WT animals of different ages under sterile conditions, and a cell suspension was obtained after grinding the tissue against a 70-μm cell strainer in PBS supplemented with 2% (vol/vol) FCS. A total of 10^6 bulk med-LN cells obtained from young (2 to 3 mo old) or aged (12 to 15 mo old) donors were injected i.v. (in PBS) into young lymphocyte-deficient (Rag2KO) animals (groups YY and OY, respectively). Echocardiography and organ harvesting were performed either at 2 mo or at 4 mo after cell transfer. To specifically address the role of T cells in these conditions, an additional group of lymphocyte-deficient animals receiving med-LN cells isolated from aged T-cell–deficient animals (TCRβKO) was included. Furthermore, a group of animals receiving cells isolated from the subiliac LNs of aged mice were also included as controls to the med-LN cell transfer. Age-matched naive Rag2KO mice were used as controls.

Echocardiography. Cardiac echocardiography was performed using the Vevo1100 system (Visualsonics) and a 38-MHz probe designed specifically for mouse studies (MS400; Visualsonics). The mice were kept under light anesthesia with isoflurane [1.5% (vol/vol)], and short-axis two-dimensional echocardiographic images were acquired at the midpapillary and apical levels of the left ventricle (LV). End-diastolic and end-systolic diameters were measured from transversal M-mode tracings, according to standard protocols that were previously established in our laboratory (13, 15). Only animals with a basal heart rate of >500 beats per minute (bpm) were included in the analysis.

Hemodynamic Measurements. Hemodynamic parameters were assessed using a pressure-volume conductance catheter positioned in the left ventricle with the closed chest configuration, as described previously (58). Briefly, the catheter (SPR-839; Millar Instruments) was inserted into the right carotid artery and then fed in a retrograde manner into the left ventricle chamber of mice under deep isoflurane anesthesia. Left-ventricular pressure-volume relationships were acquired under basal conditions using the MPVS-ultra foundation system, and data were analyzed using Labchart software (ADInstruments). The catheter was calibrated for pressure and volume (cuvette and saline methods) according to the manufacturer's instructions.

Perfusion and Organ Extraction. Animals received a heparin [40 international units (IU)] injection, and whole animal perfusion with PBS was then performed. After perfusion, the mediastinal lymph nodes were harvested, and the hearts were excised and treated as follows: The apical portion was stored in RNA later for further gene expression analysis, the medial portion was digested in collagenase type-II to obtain a cell suspension suitable for downstream flow cytometry analysis, and the basal portion (in transverse section) was frozen in optimal cutting temperature compound for later cryosectioning and immunofluorescence staining. The soleus skeletal muscle and the popliteal lymph nodes were also harvested in some experiments.

Flow Cytometry and Fluorescence-Activated Cell Sorting. A cell suspension of whole-heart samples was obtained after collagenase type-II digestion (1,000 IU/mL, 37 °C, 30 min) and then ground in Hanks' balanced salt solution containing 1% (wt/vol) BSA (BSS/BSA) using a 40-μM cell strainer, according to previous descriptions (3, 7, 13, 15). Lymph node samples were ground and prepared in BSS/BSA [5% (vol/vol) FCS]. Next, cells were stained using the following fluorescently labeled antibodies (in different combinations): anti-CD3ε (clone 145-2c11), anti-CD4 (clone RM4-5), anti-CD8 (clone 53-6.7), anti-CD11b (clone

M1/70), anti-CD25 (clone PC61), anti-CD31 (clone 390), anti-CD44 (clone IM7), anti-CD45 (clone 30-F11), anti-CD45/B220 (clone RA3-6B2), anti-CD62L (clone MEL-14), anti-CD206 (clone C068C2), Foxp3 (clone MF-14), Ki67 (clone 16a8), Ly6g (clone 1a8), Ly6c (clone HK1.4), F4/80 (clone BM8), TCRβ (clone H57-597), CCR2 (clone SA203G11), and CXCR3 (clone CXCR3-173). All antibodies were purchased from Biolegend. For intracellular cytokine stainings, bulk LN-derived cells were restimulated for 5 h in vitro in the presence of ionomycin (Sigma), phorbol-12-myristate-13-acetate (PMA, Sigma), and monensin (BD Biosciences). Measurements were made using an LSR-II or FACS Canto machine (BD), and the data were analyzed using FlowJo software.

Gene Expression Analysis. RNA was extracted from myocardial samples (apical portion) using a tissue RNA isolation kit (RNeasy mini; Qiagen). cDNA was synthesized from 300 ng of RNA using the iScript kit (Bio-Rad). A TaqMan chemistry-based quantitative PCR array panel consisting of 48 genes involved with cell stress, fibrosis, angiogenesis, and inflammation was developed to screen for shifts in myocardial gene expression profiles during aging and among genotypes (Life Technologies). Most specifically, the following assays were included in this array: house-keeping genes *Gusb* (Mm01197698_m1), *Gapdh* (Mm033002249_g1), and *Actb* (Mm00607939_s1); tissue stress/myocardial damage genes *Hspd1* (Mm00849835_g1), *Hspa4* (Mm00434038_m1), *Hspa1a* (Mm01159846_s1), *Hif1a* (Mm01198376_m1), *Gata4* (Mm00484689_m1), *Hmox1* (Mm00468922_m1), *Tlr2* (Mm00442346_m1), *Tlr4* (Mm00445273_m1), *Myd88* (Mm00440338_m1), *Casp1* (Mm00438023_m1), *Nfkb* (Mm00476361_m1), *Rela p65* (Mm00501346_m1), *Myh6* (Mm00440359_m1), *Myh7* (Mm01319006_g1), *Anp* (Mm00435329_m1), and *Adrb1* (Mm00431707_s1); proinflammatory genes *Il1b* (Mm00434228_m1), *Il6* (Mm00446190_m1), *Tnf* (Mm99999068_m1), *Ifng* (Mm01168134_m1) *Il17a* (Mm00439618_m1), *Nos2* (Mm00440488_m1), *Ccl2* (Mm00441242_m1), *Ccl5* (Mm01302427_m1), *Nox1* (Mm00549170_m1), *Cxcl13* (Mm04214185_s1), and *Cd80* (Mm00711660_m1); antiinflammatory genes *Il10* (Mm00439614_m1), *Mrc1* (Mm00485148_m1), *Foxp3* (Mm00475162_m1), *Pparg* (Mm01184322_m1), and *Pdl1* (Mm00452054_m1); and angiogenesis/extracellular matrix remodeling genes *Vegfa* (Mm00437304_m1), *Vwf* (Mm00550376_m1), *Col3a1* (Mm01254476_m1), *Col1a1* (Mm00801666_g1), *Mmp2* (Mm00439498_m1), *Mmp9* (Mm00442991_m1), *Agtra1* (Mm00616371_m1), *Tgfb1* (Mm01178820_m1), *Tgfb3* (Mm00436960_m1), *Timp1* (Mm00441818_m1), *Timp2* (Mm00441825_m1), *Spp1* (Mm00436767_m1), and *Vim* (Mm01333430_m1). The qPCR array reactions were run using pooled samples (three per group) with similar housekeeping gene expression levels (ABI7500; Life Technologies). Based on the array results, the most relevant target genes were further validated after running qPCR reactions with individual samples (five to eight per group, iCycler machine; Bio-Rad). Target gene mRNA levels were normalized to glyceraldehyde-3-phosphate dehydrogenase (GAPDH).

Histology. Cryosections (5 to 8 μm) were fixed in 4% (wt/vol) formaldehyde in PBS, blocked with goat serum [3% (vol/vol), 30 min], and then stained with antibodies against specific leukocyte subsets, according to standard protocols that were previously established in our laboratory (13, 15). Depending on the experimental setup, macrophages (CD68, clone MCA1957), B cells (B220, clone RA3-6B2), and T cells (CD3ε, clone 145-2c11; CD4, clone GK1.5; or CD8a, clone 53-6.7) were stained within the healthy myocardium. Phalloidin-Atto488 was used to stain fibrillar actin, indicating the cardiomyocyte background, wheat germ agglutinin (WGA) was used to stain the cardiomyocytes' cell surface, and DAPI was used for nuclear counterstaining. Fluorescence images were acquired using an epifluorescence microscope (model Axioskop 2 plus; Zeiss) coupled to a high-resolution camera (AxioCam HRc; Zeiss) and processed using Zen lite (Zeiss) or ImageJ (NIH) software.

Light-Sheet Microscopy. Light-sheet fluorescence microscopy (LSFM) was performed for cardiac samples according to protocols previously established by Heinze and coworkers (59). Briefly, excised hearts were perfused with PBS and then 4% (wt/vol) formaldehyde in PBS via the aorta. Next, the tissue was bleached [15% (wt/vol) H_2O_2 in methanol], stained with anti-CD45-Alexa647 (clone 30-F11) for at least 3 d, and then cleared (1:3 benzyl alcohol/benzyl acetate). Sequential multicolor stacks (1-mm total Z stack, 5-μm interval between images) were acquired using either 5× or 20× objective lenses, and the data were analyzed using Imaris software (Bitplane).

Detection of Autoantibodies. The presence of circulating heart-specific autoantibodies was assessed histologically, as previously described (60). Briefly, histological sections of hearts obtained from B-cell–deficient (hence Ig-deficient) animals were prepared as above-mentioned, and incubated with the plasma obtained from different animal groups (diluted 1:20). After washing steps, the autoantibodies reacting against cardiac antigens were detected using anti-mouse IgM-Alexa555 and anti-mouse IgG-Alexa488 antibodies (Thermo Scientific). The cardiomyocytes' cell surface was stained with WGA-Alexa647. Fluorescent images were acquired using the same exposure time. Myosin-specific autoantibodies were measured by indirect Elisa as previously described (61).

Study Approval. All animal experiments were reviewed and approved by the following local authorities: Regierung von Unterfranken Wuerzburg, Landesverwaltungsamt Halle, the ethical committee of the Instituto Gulbenkian de Ciência, and the Portuguese Veterinary General Division.

Statistics. The graphs represent the mean ± SEs of mean (SEM) obtained from *n* animals (the exact numbers are indicated in each figure legend). Statistical analyses were performed using GraphPad Prism software, as described in each figure legend. A P value of <0.05 was considered statistically significant.

ACKNOWLEDGMENTS. We greatly appreciate the excellent technical assistance of B. Bayer, H. Wagner, C. Linden, S. Umbenhauer, S. Koch, and C. Pilowski; and the mindful discussions with T. Hünig, A. Coutinho, and N. Vaz. This study was supported by grants from the Bundesministerium für Bildung und Forschung (BMBF01 EO1004) (to S.F.). U.H., S.F., and K.G.H. received funding from the German Research Foundation (DFG SFB688, TP A10, and B07). G.C.R. was supported by the Brazilian National Council for Scientific and Technological Development.

1. Choi JH, et al. (2009) Identification of antigen-presenting dendritic cells in mouse aorta and cardiac valves. *J Exp Med* 206(3):497–505.
2. Bönner F, Borg N, Burghoff S, Schrader J (2012) Resident cardiac immune cells and expression of the ectonucleotidase enzymes CD39 and CD73 after ischemic injury. *PLoS One* 7(4):e34730.
3. Pinto AR, et al. (2012) An abundant tissue macrophage population in the adult murine heart with a distinct alternatively-activated macrophage profile. *PLoS One* 7(5):e36814.
4. Aurora AB, et al. (2014) Macrophages are required for neonatal heart regeneration. *J Clin Invest* 124(3):1382–1392.
5. Epelman S, et al. (2014) Embryonic and adult-derived resident cardiac macrophages are maintained through distinct mechanisms at steady state and during inflammation. *Immunity* 40(1):91–104.
6. Frantz S, Nahrendorf M (2014) Cardiac macrophages and their role in ischaemic heart disease. *Cardiovasc Res* 102(2):240–248.
7. Heidt T, et al. (2014) Differential contribution of monocytes to heart macrophages in steady-state and after myocardial infarction. *Circ Res* 115(2):284–295.
8. Lavine KJ, et al. (2014) Distinct macrophage lineages contribute to disparate patterns of cardiac recovery and remodeling in the neonatal and adult heart. *Proc Natl Acad Sci USA* 111(45):16029–16034.
9. Molawi K, et al. (2014) Progressive replacement of embryo-derived cardiac macrophages with age. *J Exp Med* 211(11):2151–2158.
10. Epelman S, Liu PP, Mann DL (2015) Role of innate and adaptive immune mechanisms in cardiac injury and repair. *Nat Rev Immunol* 15(2):117–129.
11. Smith SC, Allen PM (1992) Expression of myosin-class II major histocompatibility complexes in the normal myocardium occurs before induction of autoimmune myocarditis. *Proc Natl Acad Sci USA* 89(19):9131–9135.
12. Donermeyer DL, Beisel KW, Allen PM, Smith SC (1995) Myocarditis-inducing epitope of myosin binds constitutively and stably to I-Ak on antigen-presenting cells in the heart. *J Exp Med* 182(5):1291–1300.
13. Hofmann U, et al. (2012) Activation of CD4+ T lymphocytes improves wound healing and survival after experimental myocardial infarction in mice. *Circulation* 125(13):1652–1663.
14. Ramos GC, et al. (2012) The autoimmune nature of post-infarct myocardial healing: Oral tolerance to cardiac antigens as a novel strategy to improve cardiac healing. *Autoimmunity* 45(3):233–244.
15. Weirather J, et al. (2014) Foxp3+ CD4+ T cells improve healing after myocardial infarction by modulating monocyte/macrophage differentiation. *Circ Res* 115(1):55–67.
16. Ramos G, Hofmann U, Frantz S (2016) Myocardial fibrosis seen through the lenses of T-cell biology. *J Mol Cell Cardiol* 92:41–45.
17. Curato C, et al. (2010) Identification of noncytotoxic and IL-10-producing CD8+AT2R+ T cell population in response to ischemic heart injury. *J Immunol* 185(10):6286–6293.
18. Hofmann U, Frantz S (2016) Role of T-cells in myocardial infarction. *Eur Heart J* 37(11):873–879.
19. Hofmann U, Frantz S (2015) Role of lymphocytes in myocardial injury, healing, and remodeling after myocardial infarction. *Circ Res* 116(2):354–367.
20. Skorska A, et al. (2015) The CD4(+) AT2R(+) T cell subpopulation improves post-infarction remodelling and restores cardiac function. *J Cell Mol Med* 19(8):1975–1985.
21. Boag SE, et al. (2015) T lymphocytes and fractalkine contribute to myocardial ischemia/reperfusion injury in patients. *J Clin Invest* 125(8):3063–3076.
22. Laroumanie F, et al. (2014) CD4+ T cells promote the transition from hypertrophy to heart failure during chronic pressure overload. *Circulation* 129(21):2111–2124.

23. Nevers T, et al. (2015) Left ventricular T-cell recruitment contributes to the pathogenesis of heart failure. *Circ Heart Fail* 8(4):776–787.
24. Chen W, Frangogiannis NG (2010) The role of inflammatory and fibrogenic pathways in heart failure associated with aging. *Heart Fail Rev* 15(5):415–422.
25. Loffredo FS, Nikolova AP, Pancoast JR, Lee RT (2014) Heart failure with preserved ejection fraction: Molecular pathways of the aging myocardium. *Circ Res* 115(1): 97–107.
26. Giannoni A, Giovannini S, Clerico A (2009) Measurement of circulating concentrations of cardiac troponin I and T in healthy subjects: A tool for monitoring myocardial tissue renewal? *Clin Chem Lab Med* 47(10):1167–1177.
27. Franceschi C, et al. (2000) Inflamm-aging: An evolutionary perspective on immunosenescence. *Ann N Y Acad Sci* 908:244–254.
28. Salvioli S, et al. (2006) Inflamm-aging, cytokines and aging: State of the art, new hypotheses on the role of mitochondria and new perspectives from systems biology. *Curr Pharm Des* 12(24):3161–3171.
29. Salvioli S, et al. (2013) Immune system, cell senescence, aging and longevity: Inflamm-aging reappraised. *Curr Pharm Des* 19(9):1675–1679.
30. Carpentier M, et al. (2013) Extrathymic induction of Foxp3^{+} regulatory T cells declines with age in a T-cell intrinsic manner. *Eur J Immunol* 43(10):2598–2604.
31. Lopes-Carvalho T, Coutinho A (2013) Old dogs and new tricks: Defective peripheral regulatory T cell generation in aged mice. *Eur J Immunol* 43(10):2534–2537.
32. Shifrut E, et al. (2013) CD4(+) T cell-receptor repertoire diversity is compromised in the spleen but not in the bone marrow of aged mice due to private and sporadic clonal expansions. *Front Immunol* 4:379.
33. Burzyn D, Benoist C, Mathis D (2013) Regulatory T cells in nonlymphoid tissues. *Nat Immunol* 14(10):1007–1013.
34. Mueller SN, Gebhardt T, Carbone FR, Heath WR (2013) Memory T cell subsets, migration patterns, and tissue residence. *Annu Rev Immunol* 31:137–161.
35. Schenkel JM, Masopust D (2014) Tissue-resident memory T cells. *Immunity* 41(6): 886–897.
36. Carbone FR (2015) Tissue-resident memory T cells and fixed immune surveillance in nonlymphoid organs. *J Immunol* 195(1):17–22.
37. Park CO, Kupper TS (2015) The emerging role of resident memory T cells in protective immunity and inflammatory disease. *Nat Med* 21(7):688–697.
38. Smith F, et al. (2003) Localization of T and B lymphocytes in histologically normal adult human donor liver. *Hepatogastroenterology* 50(53):1311–1315.
39. Ziv Y, et al. (2006) Immune cells contribute to the maintenance of neurogenesis and spatial learning abilities in adulthood. *Nat Neurosci* 9(2):268–275.
40. Jiang X, et al. (2012) Skin infection generates non-migratory memory CD8+ T(RM) cells providing global skin immunity. *Nature* 483(7388):227–231.
41. Burzyn D, et al. (2013) A special population of regulatory T cells potentiates muscle repair. *Cell* 155(6):1282–1295.
42. Holzinger C, et al. (1996) Are T cells from healthy heart really only passengers? Characterization of cardiac tissue T cells. *Immunol Lett* 53(2-3):63–67.
43. Dai DF, et al. (2009) Overexpression of catalase targeted to mitochondria attenuates murine cardiac aging. *Circulation* 119(21):2789–2797.
44. Müller-Werdan U (2007) Inflammation and ageing. *Z Gerontol Geriatr* 40(5):362–365.
45. Moro-García MA, Alonso-Arias R, López-Larrea C (2013) When aging reaches CD4+ T-cells: Phenotypic and functional changes. *Front Immunol* 4:107.
46. Moro-García MA, et al. (2014) Immunosenescence and inflammation characterize chronic heart failure patients with more advanced disease. *Int J Cardiol* 174(3): 590–599.
47. Linton PJ, Dorshkind K (2004) Age-related changes in lymphocyte development and function. *Nat Immunol* 5(2):133–139.
48. Min H, Montecino-Rodriguez E, Dorshkind K (2005) Effects of aging on early B- and T-cell development. *Immunol Rev* 205:7–17.
49. Thiault N, et al. (2015) Peripheral regulatory T lymphocytes recirculating to the thymus suppress the development of their precursors. *Nat Immunol* 16(6):628–634.
50. Paiva RS, et al. (2013) Recent thymic emigrants are the preferential precursors of regulatory T cells differentiated in the periphery. *Proc Natl Acad Sci USA* 110(16): 6494–6499.
51. Clement CC, Santambrogio L (2013) The lymph self-antigen repertoire. *Front Immunol* 4:424.
52. Bergot AS, et al. (2015) TCR sequences and tissue distribution discriminate the subsets of naïve and activated/memory Treg cells in mice. *Eur J Immunol* 45(5):1524–1534.
53. Miller JF, Mitchell GF (1968) Cell to cell interaction in the immune response. I. Hemolysin-forming cells in neonatally thymectomized mice reconstituted with thymus or thoracic duct lymphocytes. *J Exp Med* 128(4):801–820.
54. Kaya Z, Leib C, Katus HA (2012) Autoantibodies in heart failure and cardiac dysfunction. *Circ Res* 110(1):145–158.
55. Jahns R, et al. (2004) Direct evidence for a beta 1-adrenergic receptor-directed autoimmune attack as a cause of idiopathic dilated cardiomyopathy. *J Clin Invest* 113(10):1419–1429.
56. Komarowska I, et al. (2015) Hepatocyte growth factor receptor c-Met instructs T cell cardiotropism and promotes T cell migration to the heart via autocrine chemokine release. *Immunity* 42(6):1087–1099.
57. Pinto AR, et al. (2014) Age-related changes in tissue macrophages precede cardiac functional impairment. *Aging (Albany NY)* 6(5):399–413.
58. Pacher P, Nagayama T, Mukhopadhyay P, Bátkai S, Kass DA (2008) Measurement of cardiac function using pressure-volume conductance catheter technique in mice and rats. *Nat Protoc* 3(9):1422–1434.
59. Brede C, et al. (2012) Mapping immune processes in intact tissues at cellular resolution. *J Clin Invest* 122(12):4439–4446.
60. Ono M, Shimizu J, Miyachi Y, Sakaguchi S (2006) Control of autoimmune myocarditis and multiorgan inflammation by glucocorticoid-induced TNF receptor family-related protein(high), Foxp3-expressing CD25+ and CD25- regulatory T cells. *J Immunol* 176(8):4748–4756.
61. Ramos GC, et al. (2009) Cell-mediated immune response to unrelated proteins and unspecific inflammation blocked by orally tolerated proteins. *Immunology* 126(3): 354–362.